Thickness Dependence of the Dzyaloshinskii-Moriya Interaction in Co_2FeAl Ultrathin Films: Effects of Annealing Temperature and Heavy-Metal Material

M. Belmeguenai,* Y. Roussigné, H. Bouloussa, S. M. Chérif, and A. Stashkevich
LSPM, CNRS-Université Paris 13, Sorbonne Paris Cité, 99 Avenue Jean-Baptiste Clément Université Paris 13, 93430 Villetaneuse, France

M. Nasui and M. S. Gabor†
Center for Superconductivity, Spintronics and Surface Science, Technical University of Cluj-Napoca, Memorandumului No. 28, RO-400114 Cluj-Napoca, Romania

A. Mora-Hernández, B. Nicholson, O.-O. Inyang, and A. T. Hindmarch
Department of Physics, Durham University, South Road, Durham DH1 3LE, United Kingdom

L. Bouchenoire
XMaS, European Synchrotron Radiation Facility, F-38000 Grenoble, France

(Received 30 October 2017; revised manuscript received 22 January 2018; published 30 April 2018)

The interfacial Dzyaloshinskii-Moriya interaction (IDMI) is investigated in Co_2FeAl (CFA) ultrathin films of various thicknesses (0.8 nm $\leq t_{CFA} \leq$ 2 nm) grown by sputtering on Si substrates, using Pt, W, Ir, and MgO buffer or/and capping layers. Vibrating sample magnetometry reveals that the magnetization at saturation (M_s) for the Pt- and Ir-buffered films is higher than the usual M_s of CFA due to the proximity-induced magnetization (PIM) in Ir and Pt estimated to be 19% and 27%, respectively. The presence of PIM in these materials is confirmed using x-ray resonant magnetic reflectivity. Moreover, while no PIM is induced in W, higher PIM is obtained with Pt when it is used as a buffer layer rather than a capping layer. Brillouin light scattering in the Damon-Eshbach geometry is used to investigate the thickness dependences of the IDMI constants from the spin-wave nonreciprocity and the perpendicular anisotropy field versus the annealing temperature. The IDMI sign is found to be negative for Pt/CFA and Ir/CFA, while it is positive for W/CFA. The thickness dependence of the effective IDMI constant for stacks involving Pt and W shows the existence of two regimes similar to that of the perpendicular anisotropy constant due to the degradation of the interfaces as the CFA thickness approaches a critical thickness. The surface IDMI and anisotropy constants of each stack are determined for the thickest samples where a linear thickness dependence of the effective IDMI constant and the effective magnetization are observed. The interface anisotropy and IDMI constants investigated for the Pt/CFA/MgO system show different trends with the annealing temperature. The decrease of the IDMI constant with increasing annealing temperature is probably due to the electronic structure changes at the interfaces, while the increase of the interface anisotropy constant is coherent with the interface quality and disorder enhancement.

DOI: 10.1103/PhysRevApplied.9.044044

I. INTRODUCTION

Recent advances in thin-film fabrication processes have led to the possibility of growing ultrathin multilayers with high-quality interfaces. Consequently, ultrathin systems incorporating heavy-metal and ferromagnet (HM and FM) stacks are currently under intensive research due to their potential applications in the field of spintronics. Indeed, various novel mechanisms and phenomena could occur in these structures such as spin Hall [1–4] and inverse spin Hall effects [5–7], spin-orbit torques [8], and interface Dzyaloshinskii-Moriya interaction (IDMI) [9,10]. The latter is an antisymmetric exchange interaction which favors noncollinear alignment of neighboring spins. The interfacial DMI can be induced by the large spin-orbit coupling of the HM in contact with ultrathin ferromagnetic materials where the inversion symmetry is broken at the surface.

*belmeguenai.mohamed@univ-paris13.fr
†mihai.gabor@phys.utcluj.ro

If the IDMI is strong enough, it should change the static as well as the dynamic properties of the system. Indeed, it converts the magnetostatically favorable Bloch wall into a chiral Néel wall [11] and induces chiral canting of spins which leads to special chiral spin textures and, in particular, to magnetic Skyrmions [12]. Skyrmions are, thus, swirling spin textures, which are topologically protected, and, therefore, they are considered potential candidates for future energy-efficient spintronic devices [13]. Skyrmions in thin films are induced by the interfacial DMI (if the DM interaction is strong enough relative to other interactions) for which there are several choices of materials. Therefore, it is essential that the IDMI is quantified in different material systems by determining its effective (D_{eff}) or surface (D_s) constants [14] using reliable techniques to engineer the desired stacks presenting the suitable IDMI constant. Furthermore, Heusler alloys, such as Co_2FeAl having extremely small damping [15], high Curie temperatures, and relatively high spin polarization are very attractive materials for spintronics. In such alloys, there are always some degrees of chemical disorder, which strongly influences many of their physical properties [16], especially the IDMI. Therefore, an annealing process is required to initiate crystallization and to induce atomic ordering. Since IDMI is sensitive to disorder, defect, and atom arrangements at the interfaces, it is of great interest for applications and fundamental research to investigate the IDMI in Heusler-based stacks. Furthermore, it is worth mentioning that it is important to control and tune the IDMI, especially for Skyrmion applications. This control of the IDMI can be done by changing the heavy-metal material and/or by the thermal treatment via sample annealing. Therefore, in addition to the IDMI heavy-metal material dependence, the effect of the annealing temperature on the IDMI should be studied, where structural and morphology changes can occur, especially for material such as Co_2FeAl. It should be mentioned that few experimental investigations using indirect techniques (field-driven domain-wall creep) for measuring the IDMI have been reported [17]. Therefore, in this paper, we address the thickness dependence of the IDMI in HM/Co_2FeAl. Special interest is given to effects of the annealing temperature (T_a) and the HM nature (where the HMs used as buffer and/or capping layers are Ir, W, and Pt) on the IDMI and the proximity-induced magnetization. For this, the Brillouin-light-scattering (BLS) technique is used. Since the IDM interaction is antisymmetric in its nature, it will lift the degeneracy of spin waves (SWs) propagating along two opposite directions perpendicular to the static magnetization. Therefore, BLS is the most direct and efficient method for DMI characterization since few parameters are required for the experimental data fit, and it can detect simultaneously SWs propagating in opposite directions. We show that Pt and Ir induce IDMI constants with similar sign while it is the opposite for W. Moreover, the IDMI constant induced by Pt decreases with the increasing annealing temperature probably due to the electronic structure changes at the interfaces.

II. SAMPLES AND EXPERIMENTAL TECHNIQUES

Co_2FeAl (CFA) thin films are grown at room temperature on a thermally oxidized Si substrate using a magnetron sputtering system with a base pressure lower than 2×10^{-8} Torr. Prior to the deposition of the CFA film, a 2-nm-thick Ta seed layer and a HM layer (the HM is 3-nm-thick Pt, 3-nm-thick Ir, or 4-nm-thick W) are deposited on the substrate. Next, the CFA films with variable thicknesses ($0.8\ \mathrm{nm} \leq t_{\mathrm{CFA}} \leq 2\ \mathrm{nm}$) are deposited at room temperature by dc sputtering under an argon pressure of 1 mTorr at a rate of 0.1 nm/s. Finally, in order to protect the structure from air exposure, the CFA layers are capped with different materials. It is worth mentioning that the nominal layer thicknesses are confirmed by x-ray reflectivity measurements. Therefore, four sets of samples are considered here: (i) Pt-buffered samples capped with $MgO(1\ \mathrm{nm})/Ta(2\ \mathrm{nm})$, (ii) W-buffered samples capped with $MgO(1\ \mathrm{nm})/Ta(2\ \mathrm{nm})$, (iii) W-buffered samples capped with Pt (3 nm), and (iv) Ir-buffered samples capped with Ti (2 nm). It should be mentioned that the W layers are grown in a highly resistive β phase [18], while the Ir and Pt layers have the expected (111) texture [19]. The choice of Ti is motivated by the necessity of using a capping material that does not induce IDMI, thus, allowing us to precisely identify the IDMI sign of Ir. This is primarily motivated by the discrepancy between *ab initio* calculations and previous BLS measurements on this sign [20]. Moreover, the CFA films grown on Si substrates have polycrystalline structure and do not display any in-plane preferential growth direction [21]. In the heterostructures investigated here, only the HM layer induces DMI in the CFA ultrathin layers. The measurements presented here are performed at room temperature.

Hysteresis loops for perpendicular and parallel to the films' plane-applied magnetic fields are measured for all samples by a vibrating sample magnetometer (VSM). Then, the static magnetic parameters including the intrinsic value of the saturation magnetization M_s are deduced. The in-plane angular dependence of the hysteresis loops does not reveal the presence of the usual fourfold magnetocrystalline anisotropy of CFA [16], confirming the absence of any in-plane preferential growth direction. BLS, in Damon-Eshbach (DE) geometry, where the IDMI effect on the SWs nonreciprocity is maximal [22], is used to determine the IDMI constants for each sample. For this, a magnetic field sufficiently high to warrant the saturation of the magnetization in the film plane is applied perpendicular to the incidence plane. BLS spectra are then measured after counting photons up to 19 h (especially for the highest incidence angles) for different wave-vector values

($k_{SW} = [(4\pi)/\lambda] \sin\theta$, where θ is the incidence angle and $\lambda = 532$ nm is the laser wavelength). The Stokes (S) and anti-Stokes (AS) frequencies detected simultaneously are then determined from Lorentzian fits to the BLS spectra.

X-ray resonant magnetic reflectivity (XRMR) [23] measurements are made on the XMaS beam line at the European Synchrotron Radiation Source. The x-ray energy is tuned close to the L_3 absorption edge of either Pt or Ir, and a reversible, approximately 90% circularly polarized beam is induced using a diamond phase plate. The reflected intensity $I^{+(-)}$ corresponding to beam helicity parallel (antiparallel) to the saturating in-plane magnetic field applied in the scattering plane is measured as a function of the scattering angle 2θ. The derived asymmetry $(I^+ - I^-)/(I^+ + I^-)$ is sensitive to proximity-induced magnetization (PIM) in the heavy-metal layer and is expected to reverse sign when the magnetic field is reversed. The asymmetry is uniformly zero in the absence of PIM.

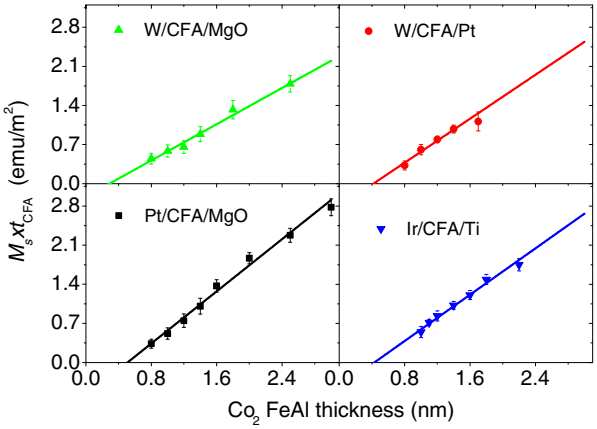

FIG. 1. Saturation magnetic moment per unit area versus Co_2FeAl thickness. Co_2FeAl thin films are grown on Si substrates with various buffer and capping materials. Symbols refer to the VSM measurements and solid lines are the linear fits.

III. RESULTS AND DISCUSSION

Figure 1 shows the Co_2FeAl thickness dependences of the saturation magnetic moment per unit area for the four sets of samples incorporating the various capping and buffer HM layers. The magnetization at saturation (M_s) and the magnetic dead-layer thickness (t_d) are straightforwardly determined from the linear fits of these data: the slope gives the saturation magnetization, while the horizontal axis intercept gives the extent of the dead layer. The thicknesses of the magnetic dead layer are found to be 0.29, 0.42, 0.51, and 0.43 nm for W/CFA/MgO, W/CFA/Pt, Pt/CFA/MgO, and Ir/CFA/Ti, respectively (see Table I). The magnetic dead layer is mainly due to intermixing at the HM/CFA interface and a possible oxidation at the CFA/MgO interface. The largest magnetic dead-layer thickness is observed for Pt/CFA/MgO and the smallest one for W/CFA/MgO, suggesting more interdiffusion from the interface Pt/CFA than the W/CFA. The origin of this layer and its compatibility with IDMI is discussed in more detail below. The M_s values shown in Table I change substantially with the stacks. The largest magnetization value ($M_s = 1167 \pm 70$ emu/cm^3) is observed for Pt/CFA/MgO and the smallest one for W/CFA/MgO ($M_s = 811 \pm 50$ emu/cm^3). For W/CFA/Pt and Ir/CFA/Ti, the M_s values are 983 ± 50 and 1063 ± 55 emu/cm^3, respectively. While the M_s of W/CFA/MgO is comparable to that of MgO/CFA/MgO ($M_s \sim 850 \pm 50$ emu/cm^3) [16], clear enhancement of M_s is observed for the other sets of samples (W/CFA/Pt, Ir/CFA/Ti, and Pt/CFA/MgO), most likely due to the proximity-induced magnetization in Pt and in Ir. This change in the film magnetization (with respect to that of MgO/CFA/MgO) corresponds to 15%, 25%, and 37% for W/CFA/Pt, Ir/CFA/Ti, and Pt/CFA/MgO, respectively, which are in good agreement with the reported values for the Ir/Co and Pt/Co [24] systems. Indeed, Ryu *et al.* [24] have experimentally observed magnetization changes of 100 and 170 emu/cm^3 for Ir/Co/Ni/Co and Pt//Co/Ni/Co with respect to that of Ir/Au/Co/Ni/Co and Pt/Au/Co/Ni/Co, respectively, which they have attributed to PIM. It is worth mentioning that no PIM is induced in W since the magnetization at the saturation of W/CFA/MgO is comparable to that of MgO/CFA/MgO. Moreover, the Pt/CFA interface provides

TABLE I. Parameters obtained from the best fits of the thickness dependences of the magnetic moment per area unit, the effective magnetization, and the effective IDMI constant of the CFA thin films grown on Si substrates using various capping and buffer layers and annealed at different temperatures.

Stack	W/CFA/MgO	W/CFA/Pt	Pt/CFA/MgO			Ir/CFA/Ti
T_a (deg)	RT	RT	RT	250 °C	400 °C	RT
t_d (nm)	0.29	0.42	0.51	0.43	0.38	0.43
M_s(emu/cm^3)	811	983	1167	1200	1220	1063
D_s(pJ/m)	0.21	0.74	−0.92	−0.85	−0.61	−0.33
K_v (MJ/m^3)	−0.31	−0.12	−0.2	−0.55	−0.27	−0.1
K_s (mJ/m^2)	0.684	0.224	0.91	1.14	1.25	0.39

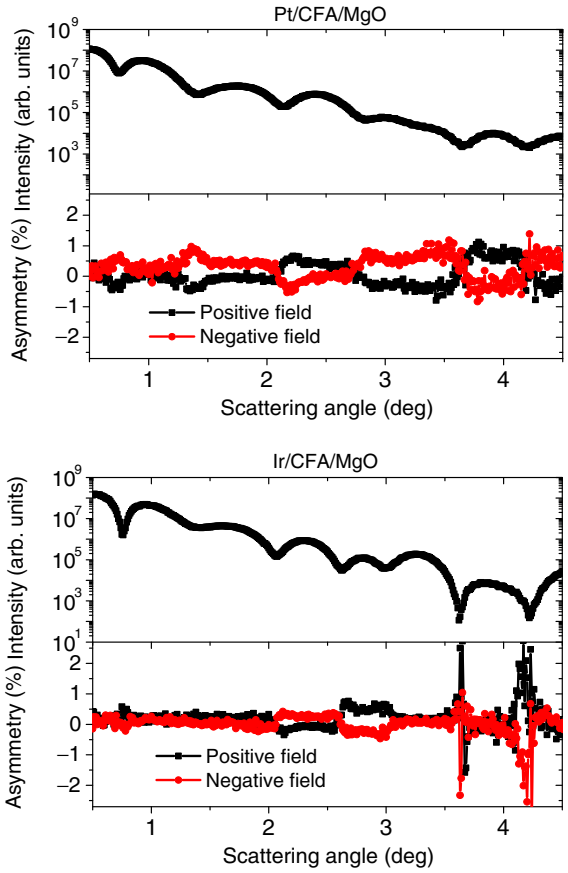

FIG. 2. Specular reflectivity and spin asymmetry data obtained from the x-ray resonant magnetic reflectivity measurements of Pt/CFA(2 nm)/MgO and Ir/CFA(2 nm)/MgO.

higher PIM compared to the CFA/Pt interface. To illustrate whether PIM exists in the different HM materials, XRMR measurements are performed. Figure 2 shows XRMR reflected intensity and asymmetry for the Ir/CFA(2 nm)/MgO and Pt/CFA(2 nm)/MgO structures. The reflected intensity (upper) has sharper features for the Ir/CFA/MgO structure compared to the Pt/CFA/MgO structure, suggesting slightly sharper structural interfaces in the Ir/CFA/MgO structure: the Ir/CFA interface appears sharper than the Pt/CFA interface. This is in good agreement with the smaller dead-layer thickness in Ir/CFA/Ti revealed by VSM. The features in the XRMR asymmetry for the Pt/CFA/MgO and Ir/CFA/MgO are generally similar except for their amplitude; the asymmetry signal is generally more pronounced in the Pt/CFA/MgO structure, which indicates a slightly larger PIM in Pt than in Ir adjacent to CFA, consistent with the VSM results in Fig. 1. The x-ray measurement does not allow us to measure at the W resonance energy, and, thus, the absence of the PIM in W/CFA/MgO films is inferred from the VSM measurements that we mentioned above. The presence of PIM in the Pt and Ir layers confirms that the measured reduction in magnetization of CFA at the interface with HM is not the result of a magnetically dead layer but rather a region of reduced

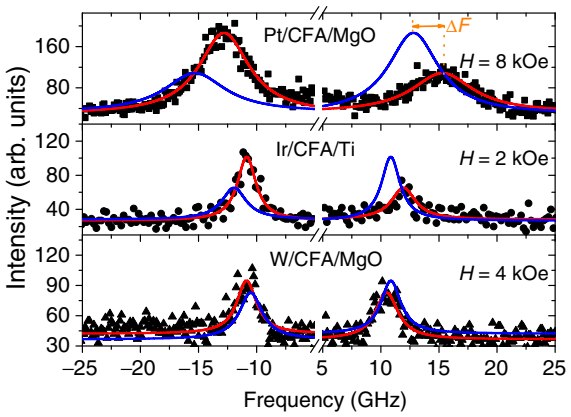

FIG. 3. BLS spectra measured for $Pt/Co_2FeAl(1.2\ nm)/MgO$, $W/Co_2FeAl(1.2\ nm)/MgO$, and $W/Co_2FeAl(1.2\ nm)/Pt$ films grown on Si at 8, 4, and 2 kOe in-plane applied field, respectively, and for a characteristic light incidence angle corresponding to $k_{SW} = 20.45\ \mu m^{-1}$. Symbols refer to the experimental data and solid lines are the Lorentzian fits. Fits corresponding to negative applied fields (blue lines) are presented for clarity and direct comparison of the Stokes and anti-Stokes frequencies.

magnetization in the vicinity of the interface with HM; a magnetic dead layer will not produce PIM in the adjacent heavy metal.

Figure 3 shows the typical BLS spectra for the W/CFA (1.2 nm)/MgO, Ir/CFA(1.2 nm)/Ti, and Pt/CFA (1.2nm)/MgO samples for $k_{SW} = 20.45\ \mu m^{-1}$ ($\theta = 60°$) and for different applied fields larger than the saturation field which is sample dependent. Note the lower signal-to-noise ratio for the W/CFA/MgO, suggesting the lesser quality of CFA grown on W. The spectra reveal the existence of both S and AS spectral lines. A pronounced difference between the frequencies of the S (left line of the spectra) and AS (right line of the spectra) modes ($\Delta F = F_S - F_{AS}$) is revealed by the BLS spectra. This frequency mismatch is HM dependent: for fixed CFA thickness, the larger shift is obtained for Pt/CFA/MgO while W/CFA/MgO provides the smallest value. Moreover, ΔF is positive for W/CFA/MgO and negative for Ir/CFA/Ti and Pt/CFA/MgO due to the interfacial DMI induced by Pt, Ir, and W, as demonstrated previously [14,20,25]. Figure 4(a) shows the k_{SW} dependence of ΔF for the four sets of CFA thin films of various thicknesses, where a clear linear behavior can be observed. Note the negative sign of ΔF for Pt/CFA/MgO and Ir/CFA/Ti and the positive sign for W/CFA/MgO and W/CFA/Pt suggesting that in addition to the opposite sign of the IDMI induced by W and Pt, the Pt buffer (capping) layer induces a negative (positive) IDMI effective constant. This sign inversion with respect to the stack order confirms the interfacial origin of the DMI and is consistent with the three-site indirect exchange mechanism [26,27] proposed previously, thus, confirming our previous observations [28]. The k_{SW} dependence of the frequency difference is given by [28]

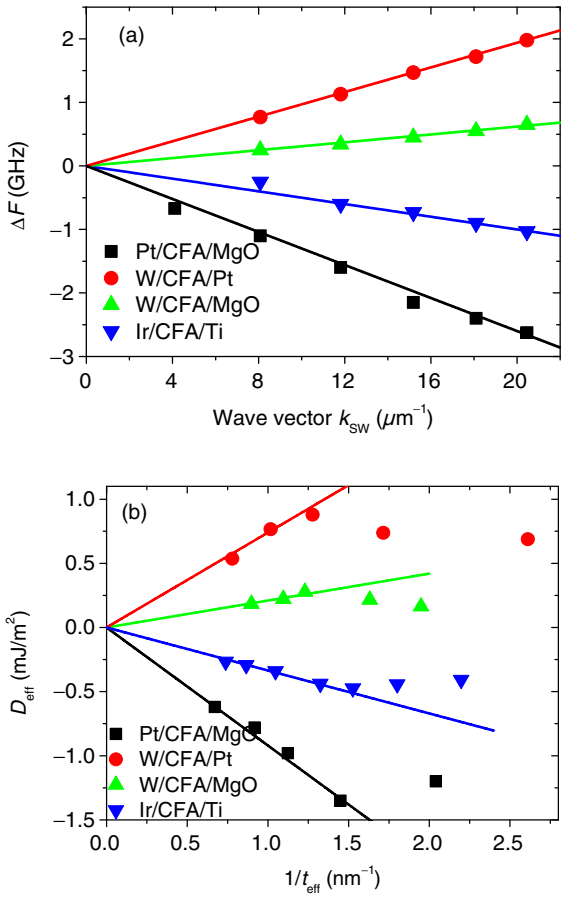

FIG. 4. (a) Wave-vector (k_{SW}) dependence of the experimental frequency difference ΔF of Pt/Co_2FeAl(1.2 nm)/MgO, W/Co_2FeAl(1.2 nm)/MgO, W/Co_2FeAl(1.2 nm)/Pt, and Ir/Co_2FeAl(1.2 nm)/Ti stacks grown on Si substrates. Symbols are experimental data and solid lines refer to the linear fit using Eq. (1) and the magnetic parameters in the main text. (b) Variation of the effective IDMI constant (D_{eff}) versus the reciprocal effective thickness of Co_2FeAl films in the four sets of stacks with various buffer and capping layers. Symbols refer to measurements and solid lines are the linear fits. D_{eff} values are obtained from fits of k_{SW} dependence of ΔF via Eq. (1) and using the magnetic parameters given in the main text.

$$\Delta F = F_S - F_{AS} = \frac{2\gamma}{\pi M_s} D_{eff} k_{SW} = \frac{2\gamma}{\pi M_s} \frac{D_s}{t_{FM}} k_{SW}. \quad (1)$$

From the slopes of the k_{SW} dependences of ΔF, the effective IDMI constants are extracted using Eq. (1) with the gyromagnetic ratio $\gamma/(2\pi) = 29.2$ GHz/T (determined previously [15,21] from ferromagnetic resonance measurements) and the above-mentioned values of M_s. The variation of D_{eff} versus the reciprocal CFA effective thickness defined as $1/t_{eff} = 1/(t_{CFA} - t_d)$ is shown in Fig. 4(b). Note the deviation from theoretical linearity, as the CFA nominal thickness approaches a critical thickness which is stack dependent: two regimes of different sign slopes can be distinguished. In the second regime corresponding to thinner CFA films with respect to the critical thickness, ΔF unexpectedly decreases with the thickness, suggesting a degradation of the interfaces for ultrathin films. The linear fit of the data of Fig. 4(b) for the CFA thickness where the theoretical relation between D_{eff} and D_s given by Eq. (1) is respected leads to $D_s = -0.33$, -0.92, 0.21, and 0.74 pJ/m for Ir/CFA/Ti, Pt/CFA/MgO, W/CFA/MgO, and W/CFA/Pt, respectively. These values are significantly lower than that of the Pt/Co/AlO_x systems [14], but they have the same sign as Pt/Co and confirm the recent results of Kim *et al.* [20] for Ir/Co. It is worth remembering that the positive sign of the IDMI constant for W/CFA/MgO and the good agreement with the obtained value of W/$Co_{20}Fe_{60}B_{20}$/SiO_2 ($D_s = 0.21$ pJ/m) [29]. Because of the opposite sign of the IDMI constants of W/CFA/MgO and Pt/CFA/MgO, one expects additive IDMI constants if the CFA is sandwiched by W and Pt. However, the weak obtained value of D_s for the W/CFA/Pt systems ($D_s = 0.74$ pJ/m) leads to an IDMI surface constant of 0.53 pJ/m for the CFA/Pt interface. This suggests the lesser quality of this latter interface compared to the Pt/CFA one, or possibly a different atomic configuration of the Pt capping layer.

We also investigate the thickness dependence of the effective magnetization defined as $\mu_0 M_{eff} = \mu_0(M_s - H_k) = \mu_0 M_s - [(2K_\perp)/(M_s)]$, where H_k and $K_\perp$ are the perpendicular uniaxial anisotropy field and the anisotropy constant, respectively. M_{eff} is obtained from the fit of the mean value of the S and AS frequencies using Eq (2):

$$F = \left(\frac{F_S + F_{AS}}{2}\right) = \mu_0 \frac{\gamma}{2\pi} \sqrt{[H + Jk_{SW}^2 + P(k_{SW} t_{FM}) M_s][H + Jk_{SW}^2 - P(k_{SW} t_{FM}) M_s + M_{eff}]}, \quad (2)$$

where H is the in-plane applied magnetic field, t_{FM} is the ferromagnetic layer thickness, μ_0 is the permeability of vacuum, and $J = [(2A_{ex})/(\mu_0 M_s)]$ with A_{ex} is the exchange stiffness constant of CFA. Figure 5 shows that for all samples, M_{eff} decreases linearly with the reciprocal effective thickness of CFA, suggesting the existence of a perpendicular interface anisotropy. Nevertheless, a pronounced nonlinear behavior is observed for the thinner

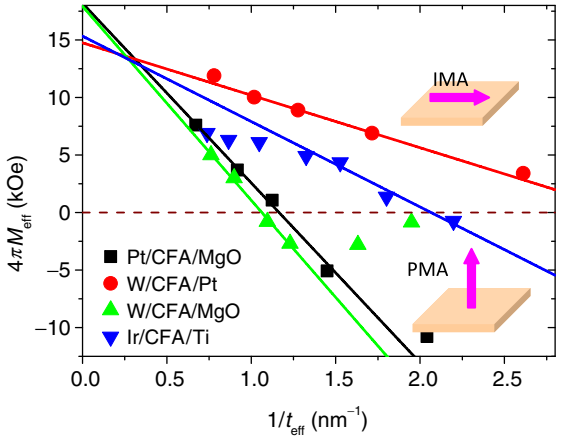

FIG. 5. Effective magnetization ($4\pi M_{\text{eff}}$) versus the effective thickness of Co_2FeAl films in Pt/Co_2FeAl/MgO, W/Co_2FeAl/MgO, W/Co_2FeAl/Pt, and Pt/Co_2FeAl/Ir grown on Si substrates. The $4\pi M_{\text{eff}}$ values are extracted from the fit of BLS measurements of the mean frequency of Stokes and anti-Stokes lines versus the wave vector using Eq. (2) and the parameters in the main text. Symbols refer to experimental data while solid lines are the linear fits. The horizontal dashed line at zero is used to indicate the thickness region where the samples are perpendicularly magnetized ($4\pi M_{\text{eff}}$ negative) and in-plane magnetized (positive $4\pi M_{\text{eff}}$). The sketch in the inset refers to thicknesses where samples present perpendicular magnetic anisotropy (PMA) and in-plane magnetic anisotropy (IMA).

CFA films in W/CFA/MgO stacks. This is in agreement with the poor spectra quality, despite a large accumulation time. This feature could be a consequence of the β-W phase for which the normal to the film is not a unique crystallographic direction [18], while the buffer Pt and Ir films are (111) oriented [19]. More generally, as we mention above and due to the interface degradation for thinner CFA films, a clear deviation from the linear behavior is observed for the stacks showing stronger interface anisotropy. The linear fit of the thickness dependence of M_{eff} (shown in Fig. 5) allows us to determine the perpendicular surface K_s and volume K_v anisotropy constants from the slope and the intercept with the vertical axis, respectively, since the perpendicular anisotropy constant $K_\perp$ obeys the relation $K_\perp = K_v + [(K_s)/t]$. The interface anisotropy constants summarized in Table I are deduced to be 0.68, 0.22, 0.91, and 0.39 mJ/m^2 for W/CFA/MgO, Pt/CFA/W, Pt/CFA/MgO, and Ir/CFA/Ti, respectively. The highest anisotropy constants are obtained for stacks involving MgO. Note also the existence of a non-negligible negative-volume perpendicular anisotropy reinforcing the in-plane magnetization easy axis estimated to be −0.31, −0.12, −0.2, and −0.1 MJ/m^3 for W/CFA/MgO, Pt/CFA/W, Pt/CFA/MgO, and Ir/CFA/Ti, respectively (see Table I). We should mention that K_v and K_s can also be determined from the VSM measurements by deducing the effective perpendicular magnetic anisotropy constant K_{eff} from the saturation field (H_s) using the relation $K_{\text{eff}} = -M_s H_s/2$ (the negative sign refers to in-plane magnetized films). The H_s value is determined from the perpendicular (in-plane) applied field hysteresis loops of the in-plane (perpendicularly) magnetized films. Phenomenologically, the K_{eff} dependence on the thickness can be separated into a volume and surface contribution as $K_{\text{eff}} \times t_{\text{eff}} = (-2\pi M_s^2 + K_v) \times t_{\text{eff}} + K_s$. The linear fit of the experimental values of $K_{\text{eff}} \times t_{\text{eff}}$ (not shown here) allows us to determine the perpendicular surface K_s and volume K_v anisotropy constants from the intercept with the vertical axis and the slope, respectively. This procedure is tested for Ir/CFA/Ti systems allowing us to deduce $K_s = 0.32$ mJ/m^2 and $K_v = -0.22$ MJ/m^3, which are in good agreement with those obtained from dynamic measurements. However, the determination of the anisotropy constants via the dynamic methods remains more precise and more suitable, and, therefore, to simplify this work, the anisotropy determination is limited to the BLS technique.

The effect of the annealing temperature on both IDMI constants and interface anisotropy is investigated for the Pt/CFA/MgO stacks showing the higher values for these quantities. The samples are annealed at 250 and 400 °C in vacuum (with a pressure lower than 3×10^{-8} Torr) for 1 h, and then they are characterized by VSM, XRMR, and BLS. The VSM measurements show that the M_s values increase slightly as the annealing temperature increases: $M_s = 1200 \pm 70$ and 1220 ± 70 emu/cm^3, respectively, for annealing temperatures of 250 and 400 °C. Although the M_s variation with respect to that of the as-deposited films is within the error bar, we note the slight enhancement of the PIM contribution for annealed samples. It is worth mentioning that the magnetic dead-layer thickness decreases to 0.38 nm for the annealed films at 400 °C. We, thus, conclude on the increase of the proximity magnetization in Pt with the enhancement of the interface quality.

From the XRMR measurements of the Pt/CFA (2 nm)/MgO sample annealed at 400 °C and shown in Fig. 6, we see changes in both the reflected intensity and asymmetry after annealing, indicative of both structural and magnetic changes in the structure. At lower scattering angles below 2°, the reflectivity is largely unchanged after annealing at 400 °C, but the asymmetry signal is significantly enhanced, indicative of an increased PIM. Note that the PIM itself is small and localized close to the interface [30], such that this enhancement makes a low contribution to the M_s value measured by VSM (that is less adapted to evidence PIM). At scattering angles from around 3° upwards, we observe changes in the reflected intensity, suggesting subtle changes in the multilayer structure. The more pronounced Kiessig fringes in the annealed structure suggest a sharper interface between Pt and CFA after annealing at 400 °C, which is in agreement with the smaller

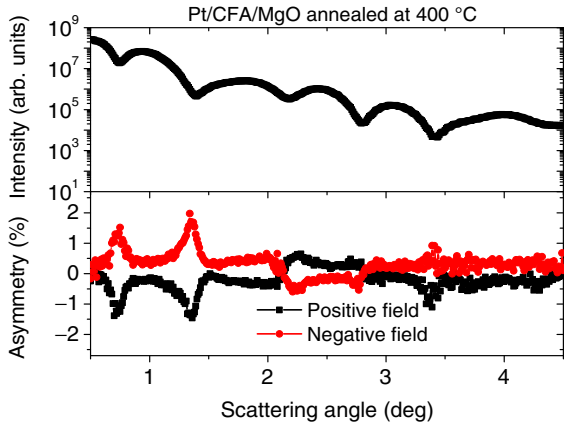

FIG. 6. Specular reflectivity and spin asymmetry data obtained from the x-ray resonant magnetic reflectivity measurements of Pt/CFA(2 nm)/MgO annealed at 400 °C.

dead-layer thickness deduced from VSM. We, thus, conclude that the increase of the proximity magnetization in Pt is related to an enhancement of the interface quality. This can be related to the reorganization of the Fe and Co atoms yielding an enhancement of Pt atom polarization as well as a structural improvement of the interfaces.

The typical BLS spectra measured for $k_{SW} = 20.45\ \mu m^{-1}$ are shown in Fig. 7 for the 1.2-nm-thick films and for the three different annealing temperatures. One can observe a significant enhancement of the signal-to-noise ratio as the annealing temperature increases. A significant decrease of the full width at half maximum linewidth (δF) as the annealing temperature increases is observed. For example, for the 1-nm-thick CFA film, the mean value of δF decreases from 5.8 GHz for the as-deposited film to 4.5 GHz for the

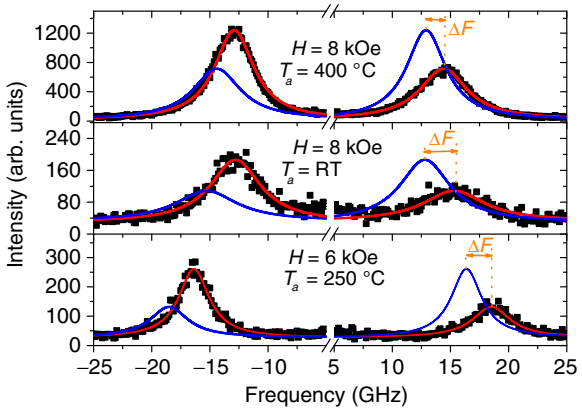

FIG. 7. BLS spectra of Pt/Co_2FeAl(1.2 nm)/MgO grown on Si and annealed at various temperatures (T_a) measured at 8 and 6 kOe in-plane applied field and for a characteristic light incidence angle corresponding to $k_{SW} = 20.45\ \mu m^{-1}$. Symbols refer to the experimental data and solid lines are the Lorentzian fits. Fits corresponding to negative applied fields (blue lines) are presented for clarity and direct comparison of the Stokes and anti-Stokes frequencies.

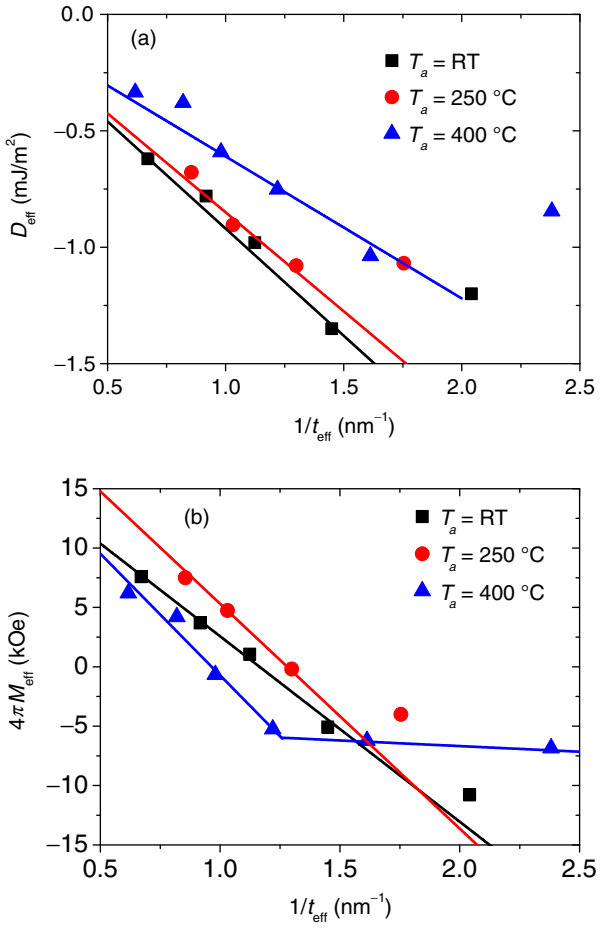

FIG. 8. Variation of the (a) effective IDMI constant (D_{eff}) and (b) effective magnetization ($4\pi M_{eff}$) versus the reciprocal effective thickness of Co_2FeAl films in Pt/Co_2FeAl/MgO stacks annealed at various temperatures (T_a). Symbols refer to measurements and solid lines are the linear fits. D_{eff} values are obtained from fits of k_{SW} dependence of ΔF using Eq. (1) and the magnetic parameters in the main text, while the $4\pi M_{eff}$ values are obtained from the fit of BLS measurements of the mean frequency of Stokes and anti-Stokes lines versus the wave vector using Eq. (2).

one annealed at 400 °C. This is in agreement with the previously obtained results, where we reported a decrease of the damping in CFA films as the annealing temperature increases [21]. Figure 8 shows the thickness dependences of D_{eff} and M_{eff} of the as-deposited and annealed samples. The films annealed at 400 °C show a significant difference with respect to the as-deposited and 250 °C annealed samples. Indeed, D_{eff} shows a noticeable decrease at $T_a = 400$ °C [Fig. 8(a)], where the significant changes in the structural chemical order and magnetic properties start to occur [16]. Furthermore, Fig. 8 reveals that D_{eff} and M_{eff} follow a linear variation which is annealing temperature dependent. Interestingly, this thickness dependence deviates from the previous linear behavior for the ultrathin (approaching 1 nm) CFA films, and the deviation becomes more pronounced for

$T_a = 400\,°C$, especially for M_{eff}. Indeed, for samples annealed at 400 °C, depending on the CFA effective thickness, two different regimes can be distinguished. For both regimes, M_{eff} decreases linearly with $1/t_{eff}$ but with different slopes: the slope is higher for $1/t_{eff} < 1.25\ nm^{-1}$. This nonlinear behavior is most probably due to the degradation of the interface for ultrathin films as the samples are annealed at higher temperatures. Therefore, to obtain a meaningful estimation of anisotropy constants for samples annealed at 400 °C, the anisotropy energies are extracted from the linear fit of the M_{eff} measurements of Fig. 8(b) for $1/t_{eff} < 1.25\ nm^{-1}$. Moreover, from the linear fit of the experimental data of Fig. 8(a), the surface IDMI constants are deduced. We find that anisotropy and IDMI constants follow opposite trends. While the interface anisotropy increases slightly with T_a (1.14 and 1.25 mJ/m^2 for $T_a = 250$ and 400 °C, respectively), D_s shows drastic decreases for the films annealed at 400 °C ($D_s = -0.85$ and $-0.61\ mJ/m^2$ for $T_a = 250$ and 400 °C, respectively). The different parameters obtained from BLS and VSM data are summarized in Table I. Note the similar trend of the PIM and surface anisotropy with the annealing temperature. The increase of the anisotropy constant is coherent with the previously observed trends in MgO/CFA/MgO [16]. It is probably due to the enhancement of the CFA/MgO surface anisotropy. While surface anisotropy results from the two interfaces, the IDMI effect is due only to the Pt/CFA interface. The IDMI is sensitive to the Co, Fe electronic structure at the interface which is highly temperature dependent. On the other hand, it is not surprising to observe different trends for the IDMI and surface anisotropy constants because the first involves only one interface, while the second involves both interfaces. The different behaviors of PIM and IDMI versus the annealing temperature probably suggests a different origin in these samples.

Finally, the simultaneous existence of the PIM, IDMI, and the magnetic dead layer could appear as incompatible. However, we think that this feature is not surprising and can be explained in the following way. It is difficult to determine the interface involved in this dead layer. However, we consider the most unfavorable configuration where the dead layer mainly lies at the interface HM/CFA. By dead layer, we mean an intermediate area of the sample between the HM and CFA layers resulting from the interdiffusion, where the magnetization is reduced but not zero. The presence of this so-called dead layer is not incompatible with the IDMI, since the IDMI results from the scattering of pure CFA electrons by HM atoms (even present in the dead layer), according to the three-site model [27]. Moreover, as shown by Tacchi *et al.* [31], the HM atoms involved in IDMI can be spread in several atomic planes (up to 2 nm depth for Pt), largely thicker than the observed dead layer in our samples. We think that the observed BLS signal mainly comes from the pure CFA layer, since the SW frequency resulting from this dead layer would be much lower due to its lower magnetization. Therefore, it is not surprising to observe this linear dependence with the reciprocal effective thickness of CFA. Furthermore, the intermixing between HM and CFA (engendering the dead layer) favors the exchange interaction with HM, thus, inducing a PIM in the HM. This simple view is compatible with the observed simultaneous increasing of the PIM and dead-layer thickness: the thicker the dead layer, the higher the PIM.

IV. CONCLUSIONS

Co_2FeAl films of various thicknesses are prepared by sputtering on Si/SiO_2 substrates using different buffer and capping layers (MgO, W, Pt, and Ir). The vibrating sample magnetometry measurements reveal that in contrast to W, the Pt- and Ir-buffered layers show a higher magnetization at saturation, possibly due to the proximity magnetization, which we show using x-ray resonant magnetic reflectivity to be induced in Pt and Ir. We also show that the Pt buffer layer induces higher proximity magnetization than the Pt capping layer. Brillouin light scattering is used in the Damon-Eshbach geometry to investigate the spin-wave nonreciprocity induced by the IDMI. It turns out that the IDMI effective constant sign and strength is material and stack-order dependent. While Pt and Ir present the same IDMI constant sign, W induces an IDMI of opposite sign. Moreover, the Pt layer providing the higher IDMI constant with respect to Ir and W seems to induce a higher IDMI effect when it is used as buffer layer rather than a capping layer. The effect of the annealing temperature on the IDMI is studied in $Pt/Co_2FeAl/MgO$ stacks, where a decrease of the IDMI constant is observed. The analysis of BLS measurements reveals the existence of perpendicular interface anisotropy which shows a different trend versus the annealing temperature from that of the IDMI constant.

ACKNOWLEDGMENTS

We would like to thank Engineering and Physical Sciences Research Council for the provision of XMaS beam time. This work is supported by the Conseil regional d'Île-de-France through the Domaines d'Intérêts Majeurs Nano-K (Brillouin light scattering Investigation of the Dzyaloshinskii-Moriya interaction in Ultrathin Layers based systems project). M. N. and M. S. G. acknowledge the financial support of Unitatea Executiva pentru Finantarea Invatamantului Superior, a Cercetarii, Dezvoltarii si Inovarii through PN-II-RU-TE-2014-1820—SPINCOD (Advanced spintronic devices for communication and data storage technologies based on Heusler compounds) research Grant No. 255/01.10.2015. A. M.-H. acknowledges fellowship support from CONACYT, B. N. acknowledges support via an EPSRC doctoral training partnership grant, and O.-O. I. acknowledges support from a Nigerian government TETFund scholarship.

[1] M. I. Dyakonov and V. I. Perel, Current-induced spin orientation of electrons in semiconductors, Phys. Lett. **35A**, 459 (1971).

[2] J. E. Hirsch, Spin Hall Effect, Phys. Rev. Lett. **83**, 1834 (1999).

[3] S. Zhang, Spin Hall Effect in the Presence of Spin Diffusion, Phys. Rev. Lett. **85**, 393 (2000).

[4] S. O. Valenzuela and M. Tinkham, Direct electronic measurement of the spin Hall effect, Nature (London) **442**, 176 (2006).

[5] L. K. Werake, B. A. Ruzicka, and H. Zhao, Observation of Intrinsic Inverse Spin Hall Effect, Phys. Rev. Lett. **106**, 107205 (2011).

[6] E. Saitoh, M. Ueda, H. Miyajima, and G. Tatara, Conversion of spin current into charge current at room temperature: Inverse spin-Hall effect, Appl. Phys. Lett. **88**, 182509 (2006).

[7] M. V. Costache, M. Sladkov, S. M. Watts, C. H. van der Wal, and B. J. van Wees, Electrical Detection of Spin Pumping due to the Precessing Magnetization of a Single Ferromagnet, Phys. Rev. Lett. **97**, 216603 (2006).

[8] S. Woo, M. Mann, A. J. Tan, L. Caretta, and G. S. D. Beach, Enhanced spin-orbit torques in Pt/Co/Ta heterostructures, Appl. Phys. Lett. **105**, 212404 (2014).

[9] I. E. Dzyaloshinskii, Thermodynamical theory of "weak" ferromagnetism in antiferromagnetic substances, Sov. Phys. JETP **5**, 1259 (1957).

[10] T. Moriya, Anisotropic superexchange interaction and weak ferromagnetism, Phys. Rev. **120**, 91 (1960).

[11] G. Chen, J. Zhu, A. Quesada, J. Li, A. T. N'Diaye, Y. Huo, T. P. Ma, Y. Chen, H. Y. Kwon, C. Won, Z. Q. Qiu, A. K. Schmid, and Y. Z. Wu, Novel Chiral Magnetic Domain Wall Structure in Fe/Ni/Cu(001) Films, Phys. Rev. Lett. **110**, 177204 (2013).

[12] G. Finocchio, F. Büttner, R. Tomasello, M. Carpentieri, and M. Kläui, Magnetic skyrmions: From fundamental to applications, J. Phys. D **49**, 423001 (2016).

[13] C. Hanneken, F. Otte, A. Kubetzka, B. Dupé, N. Romming, K. von Bergmann, R. Wiesendanger, and S. Heinze, Electrical detection of magnetic Skyrmions by tunnelling non-collinear magnetoresistance, Nat. Nanotechnol. **10**, 1039 (2015).

[14] M. Belmeguenai, J.-P. Adam, Y. Roussigné, S. Eimer, T. Devolder, J.-V. Kim, S. M. Chérif, A. Stashkevich, and A. Thiaville, Interfacial Dzyaloshinskii-Moriya interaction in perpendicularly magnetized Pt/Co/AlO_x ultrathin films measured by Brillouin light spectroscopy, Phys. Rev. B **91**, 180405(R) (2015).

[15] M. Belmeguenai, H. Tuzcuoglu, M. S. Gabor, T. Petrisor, Jr., C. Tiusan, D. Berling, F. Zighem, T. Chauveau, S. M. Chérif, and P. Moch, Co_2FeAl thin films grown on MgO substrates: Correlation between static, dynamic, and structural properties, Phys. Rev. B **87**, 184431 (2013).

[16] M. Belmeguenai, M. S. Gabor, F. Zighem, Y. Roussigné, D. Faurie, and C. Tiusan, Annealing temperature and thickness dependencies of structural and magnetic properties of Co_2FeAl thin films, Phys. Rev. B **94**, 104424 (2016).

[17] R. A. Khan, P. M. Shepley, A. Hrabec, A. W. J. Wells, B. Ocker, C. H. Marrows, and T. A. Moore, Effect of annealing on the interfacial Dzyaloshinskii-Moriya interaction in Ta/CoFeB/MgO trilayers, Appl. Phys. Lett. **109**, 132404 (2016).

[18] M. S. Gabor, T. Petrisor, Jr., R. B. Mos1, A. Mesaros, M. Nasui, M. Belmeguenai, F. Zighem, and C. Tiusan, Spin-orbit torques and magnetization switching in W/Co_2FeAl/MgO structures, J. Phys. D **49**, 365003 (2016).

[19] M. Gabor, T. Petrişor, Jr., R. B. Mos, M. Nasu, C. Tiusan, and T. Petrisor, Interlayer exchange coupling in perpendicularly magnetized Pt/Co/Ir/Co/Pt structures, J. Phys. D **50**, 465004 (2017).

[20] N.-H. Kim, J. Jung, J. Cho, D.-S. Han, Y. Yin, J.-S. Kim, H. J. M. Swagten, and C.-Y. You, Interfacial Dzyaloshinskii-Moriya interaction, surface anisotropy energy, and spin pumping at spin orbit coupled Ir/Co interface, Appl. Phys. Lett. **108**, 142406 (2016).

[21] M. Belmeguenai, H. Tuzcuoglu, M. S. Gabor, T. Petrisor, Jr., C. Tiusan, F. Zighem, S. M. Chérif, and P. Moch, Co_2FeAl Heusler thin films grown on Si and MgO substrates: Annealing temperature effect, J. Appl. Phys. **115**, 043918 (2014).

[22] V. L. Zhang, K. Di, H. S. Lim, S. C. Ng, M. H. Kuok, J. Yu, J. Yoon, X. Qiu, and H. Yang, In-plane angular dependence of the spin-wave nonreciprocity of an ultrathin film with Dzyaloshinskii-Moriya interaction, Appl. Phys. Lett. **107**, 022402 (2015).

[23] R. M. Rowan-Robinson, A. A. Stashkevich, Y. Roussigné, M. Belmeguenai, S.-M. Cherif, A. Thiaville, T. P. A. Hase, A. T. Hindmarch, and D. Atkinson, The interfacial nature of proximity-induced magnetism and the Dzyaloshinskii-Moriya interaction at the Pt/Co interface, Sci Rep. **7**, 16835 (2017).

[24] K.-S. Ryu, S.-H. Yang, L. Thomas, and S. S. P. Parkin, Chiral spin torque arising from proximity-induced magnetization, Nat. Commun. **5**, 3910 (2014).

[25] R. Soucaille, M. Belmeguenai, J. Torrejon, J.-V. Kim, T. Devolder, Y. Roussigné, S.-M. Chérif, A. A. Stashkevich, M. Hayashi, and J.-P. Adam, Probing the Dzyaloshinskii-Moriya interaction in CoFeB ultrathin films using domain wall creep and Brillouin light spectroscopy, Phys. Rev. B **94**, 104431 (2016).

[26] A. Fert, V. Cros, and J. Sampaio, Skyrmions on the track, Nat. Nanotechnol. **8**, 152 (2013).

[27] A. Fert, Magnetic and transport properties of metallic multilayers, Mater. Sci. Forum **59–60**, 439 (1990).

[28] M. Belmeguenai, M. S. Gabor, Y. Roussigné, A. Stashkevich, S.-M. Chérif, F. Zighem, and C. Tiusan, Brillouin light scattering investigation of the thickness dependence of Dzyaloshinskii-Moriya interaction in $Co_{0.5}Fe_{0.5}$ ultrathin films, Phys. Rev. B **93**, 174407 (2016).

[29] A. K. Chaurasiya, C. Banerjee, S. Pan, S. Sahoo, S. Choudhury, J. Sinha, and A. Barmanb, Direct observation of interfacial Dzyaloshinskii-Moriya interaction from asym-

metric spin-wave propagation in W/CoFeB/SiO_2 heterostructures down to sub-nanometer CoFeB thickness, Sci. Rep. **6**, 32592 (2016).

[30] T. Kuschel, C. Klewe, J.-M. Schmalhorst, F. Bertram, O. Kuschel, T. Schemme, J. Wollschläger, S. Francoual, J. Strempfer, A. Gupta, M. Meinert, G. Götz, D. Meier, and G. Reiss, Static Magnetic Proximity Effect in Pt/$NiFe_2O_4$ and Pt/Fe Bilayers Investigated by X-Ray Resonant Magnetic Reflectivity, Phys. Rev. Lett. **115**, 097401 (2015).

[31] S. Tacchi, R. E. Troncoso, M. Ahlberg, G. Gubbiotti, M. Madami, J. Åkerman, and P. Landeros, Interfacial Dzyaloshinskii-Moriya Interaction in Pt/CoFeB Films: Effect of the Heavy-Metal Thickness, Phys. Rev. Lett. **118**, 147201 (2017).